Proceedings of the IASS 2024 Symposium
Redefining the Art of Structural Design
August 26-30, 2024, Zurich Switzerland
Philippe Block, Giulia Boller, Catherine DeWolf,
Jacqueline Pauli, Walter Kaufmann (eds.)

Effect of cable-membrane contact on mechanical properties of air-supported membrane structures

Xinyu XU[a,*], Xiaoying SUN[a]

[a,*] Key Lab of Structures Dynamic Behavior and Control of China Ministry of Education, Harbin Institute of Technology
73 Huanghe Road, Nangang District, Harbin, Heilongjiang, China
xxy_hit99@163.com

Abstract

Cable net reinforced large-span air-supported membrane structures are widely used in stadiums and coal sheds due to their low cost, short construction period, and excellent seismic performance. During the service period, it is prone to wind-induced damage, thus how the membrane and cable work together under the action of fluctuating wind load is worthy of attention. Therefore, the cable net reinforced air-supported membrane structure with rectangular projection is regarded as the research object of this study. The nonlinear finite element analysis method of the air-supported membrane structure considering the cable-membrane contact effect is established, which can simulate the working state of relative slippage and separation between cable and membrane. Then, according to the wind tunnel test results, the static response of the air-supported membrane structure under mean wind load is analyzed. The results show that the cable-membrane separation phenomenon occurred in the windward area, causing the membrane displacement to become larger. Both membrane stress and cable stress become more uniform, and the stress changes more uniformly and continuously.

Keywords: air-supported membrane structure, cable–membrane contact, static wind response analysis

1. Introduction

In recent years, air-supported membrane structures have been extensively applied due to their numerous advantages. As the requirements for functional usage intensify, the span of air-supported membrane structures correspondingly expands, which frequently incorporate reinforced cable nets to collaboratively resist wind loads.

The teams led by Chen [1] and Li [2] have independently developed and installed structural health monitoring systems for air-supported membrane structures, obtaining authentic wind-induced responses during typhoon conditions. These findings can effectively inform the theoretical research and engineering design of air-supported membrane structures. Yan et al. [3], [4], [5] have undertaken investigations into the mechanical behavior of air-supported membrane structures under wind loads, employing both rigid model tests and aeroelastic model tests, with a focus on the impact of a multitude of structural parameters. In addition, the finite element method (FEM), as a convenient and effective approach, is also extensively employed in the research of air-supported membrane structures. Fang et al. [6], [7] have conducted numerical simulations on air-supported membrane structures with various geometric shapes, including semi-cylindrical, hemispherical, and truncated spherical forms. These studies have clarified the impact of numerous parameters on the mechanical performance of the membrane structures, such as membrane thickness, internal pressure, wind directions, and height-span ratio. Furthermore, they have proposed recommended values for the wind vibration coefficient. However, the aforementioned studies exhibit limitations, as they have not considered the impact of cable-membrane contact interaction. This interaction involves the phenomena of relative slippage and

separation between the cable net and the membrane surface under the influence of wind loads, which in turn affects the mechanical performance of the structure. Currently, only the research conducted by Wang [8] and He [9] has taken into account the effect of cable-membrane contact. The findings indicate that considering cable-membrane contact yields a more rational structural response.

2. Finite element method of air-supported membrane structure considering cable-membrane contact

Previous numerical simulation studies on cable net reinforced air-supported membrane structures often employed a cable-membrane binding FE model, which treated the membrane surface and cable net as a unified entity, considering only their equivalent stiffness and overlooking the interaction between them. Under wind load conditions, the potential for cable-membrane relative slippage and separation exists. To simulate the operational state of the two components more accurately, this section introduces a nonlinear finite element method that incorporates the effects of cable-membrane contact and aims to enhance the fidelity of the simulations, obtaining the complex interactions within the structure.

2.1 Finite element method of air-supported membrane structure

The FE model of the cable net reinforced air-supported membrane structure is composed of membrane elements and cable elements. It operates under the following fundamental assumptions during the calculation process:(1) The tensioning of cables and membranes constitutes a small strain problem, existing in a fully elastic stage, conforming to the generalized Hooke's law. (2) Cables and membranes can only withstand tensile forces, the membrane material lacks out-of-plane stiffness. (3) The membrane consistently maintains orthotropic anisotropy, and the cross-sectional area of the cables remains unchanged, unaffected by deformation. (4) The contact interaction is defined between cables and membranes to simulate the working states such as relative slippage and separation.

The load-deformation process of the cable net reinforced air-supported membrane structure represents a geometrically nonlinear process characterized by large deformations and small strains. According to nonlinear finite element theory, the fundamental finite element equation is provided. Equation (1) represents the equilibrium equation of the element:

$$\left(K_L^e + K_{NL}^e\right)\Delta U^e = R^e - F^e \tag{1}$$

where K_L^e is linear stiffness matrix, K_{NL}^e is nonlinear stiffness matrix caused by large deformation and initial prestress, ΔU^e is node displacement vector of an element, R^e is load vector of an element, F^e is equivalent load vector of nodes.

The assembly of the equilibrium equations for the cable and membrane elements obtains the equilibrium equation for the air-supported membrane structure within the global coordinate system, as shown in Equation (2):

$$\left(K_L + K_{NL}\right)\Delta U = R - F \tag{2}$$

The geometry of the air-supported membrane structure is influenced by both internal pressure and prestress. In the finite element calculation, the internal pressure is applied in the form of a uniformly distributed surface load on the membrane elements. The prestress is applied to the membrane and cable elements using the temperature reduction method and the initial strain method respectively. The analysis software employed is ANSYS APDL.

Before conducting a load analysis, it is essential to perform an initial form analysis of the air-supported membrane structure. This process primarily consists of two parts: first, the form finding method using a small Young's modulus, and second, the state finding method through self-equilibrating iteration (Figure 1). The initial shape and stress state of the air-supported membrane structure are obtained through the analysis.

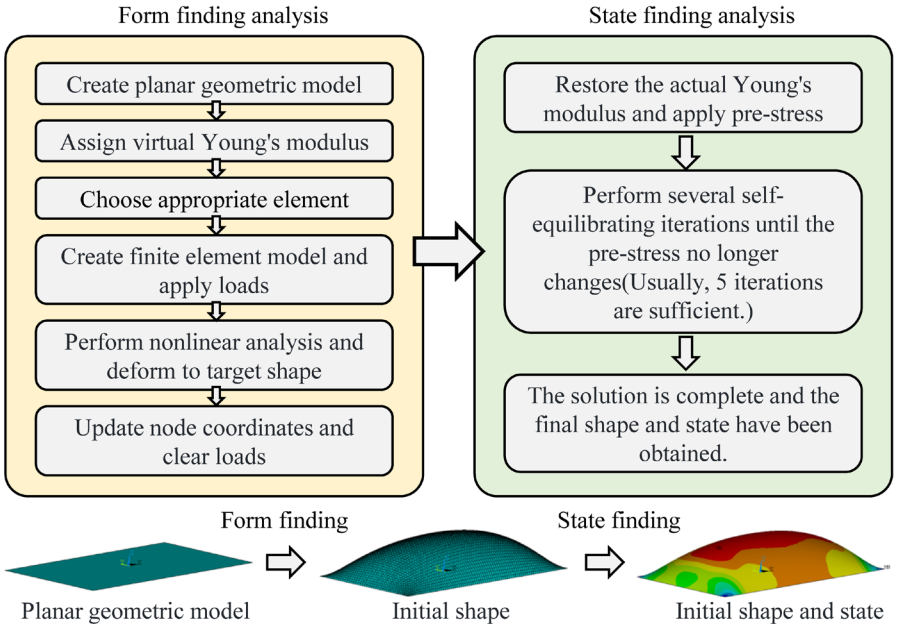

Figure 1 Initial form analysis flow

In both initial form analysis and load analysis, it is imperative to prevent failure conditions such as wrinkling of the membranes and slackening of the cables. Therefore, the failure states of membranes and cables are determined and addressed respectively during calculation.

Failure of the membrane element is determined based on the principal stresses: if the principal stresses in both principal axes are not less than zero, it indicates that the entire structure is operating normally with no wrinkles present. If any principal stress is less than zero, it signifies local wrinkling has occurred. The internal pressure and prestress must be adjusted and then the structure is recalculated. The determination of cable failure is based on the axial force, if the axial force of any cable element is less than zero, it indicates that the cable is slack. It is necessary to adjust the initial conditions and recalculate.

2.2 Cable-membrane contact setting

The finite element analysis method considering cable-membrane contact is proposed to improve the accuracy of air-supported membrane structure simulation. This method is utilized to simulate the phenomena of cable-membrane relative slippage and separation. The FE model established using this method is referred to as the cable-membrane contact model, or simply the contact model. In contrast, the FE model commonly used in previous studies, which treats the cable and membrane as a single entity and considers only its equivalent stiffness, is known as the cable-membrane binding model, or the binding model for short.

Compared to the binding model, the most significant difference in the contact model is the definition of contact action between the membrane surface and the cable net. Through nonlinear calculations, the adhesion, slippage, and separation between the membrane and cable are simulated. This leads to increased complexity in the simulation, requiring substantial computational resources and presenting greater challenges in achieving convergence. The following assumptions are necessary: (1) The surfaces of the contacting bodies are continuous; (2) The contacting bodies are in a fully elastic state, conforming to Hooke's Law. (3) The friction force on the surfaces of the contacting bodies follows Coulomb's friction model.

In the contact model, the membrane is designated as the target surface and is simulated using the target element, and the cable is designated as the contact body and is simulated using the contact element. This configuration establishes a node-to-surface contact pair between the membrane and the cable, as shown in Figure 2.

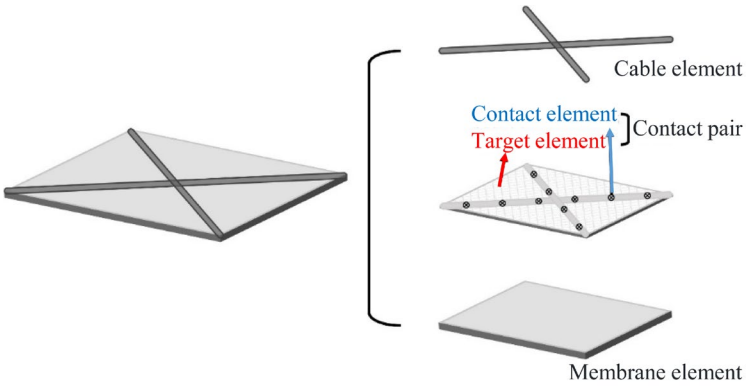

Figure 2 Schematic diagram of node-to-surface contact pair

The contact algorithm in finite element analysis is a relationship established to satisfy the contact coordination between two contacting bodies. This study adopts the augmented Lagrange method. This method first achieves contact coordination quickly based on the normal penalty stiffness, then immediately checks for penetration distance. If the penetration distance exceeds the tolerance, the normal penalty stiffness is automatically modified for the next iteration, until the penetration distance meets the requirements.

3. Wind load characteristic and finite element model

The cable net reinforced air-supported membrane structure with rectangular projection is regarded as the research object of this study, The structure's geometric dimensions are 120m x 240m x 40m, with a height-span ratio of 1:3 and an aspect ratio of 2:1. The cable net is arranged diagonally with a spacing of 6m, as shown in Figure 3.

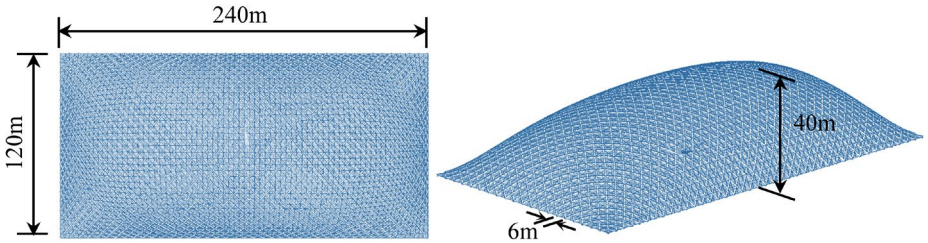

Figure 3 Schematic diagram of air-supported membrane structure

3.1 Wind load characteristic

The rigid model wind tunnel test for the air-supported membrane structure is conducted at the wind tunnel laboratory of Harbin Institute of Technology (Figure 4), resulting in the acquisition of its wind load characteristics. The study focuses exclusively on 0° wind direction, meaning the incoming wind direction is perpendicular to the direction of the longer axis of the rectangular cross-section. Based on the pressure time history data obtained from the rigid test, the time history data of the wind pressure coefficients at various measurement points on the model surface is calculated. It is stipulated here that wind pressure is considered a positive value, while wind suction is considered a negative value. Subsequently, by averaging the time history data of the wind pressure coefficients at each measurement point, the mean wind pressure coefficient for each point is obtained. The mean wind pressure coefficient contour is plotted, as shown in Figure 5.

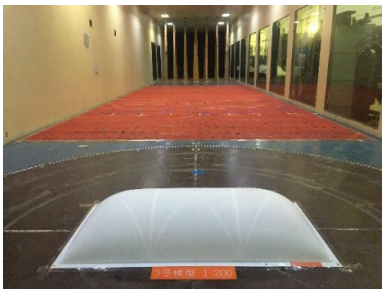

Figure 4 Test model

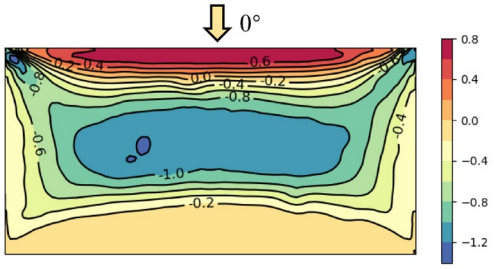

Figure 5 Mean wind pressure coefficient contour

3.2 The establishment of finite element model

In accordance with the structural information, the methods described in Section 2 are employed to establish both contact and binding models respectively. This approach facilitates the investigation of the impact of cable-membrane contact interactions on the mechanical performance of the air-supported membrane structure. The FE model incorporates four types of elements. The membrane surface employs SHELL41 element, while the cable net employs LINK10 element. In addition, the contact model uses CONTA175 and TARGE170 elements to establish contact pairs. The two types of FE models are shown in Figure 6 and Figure 7.

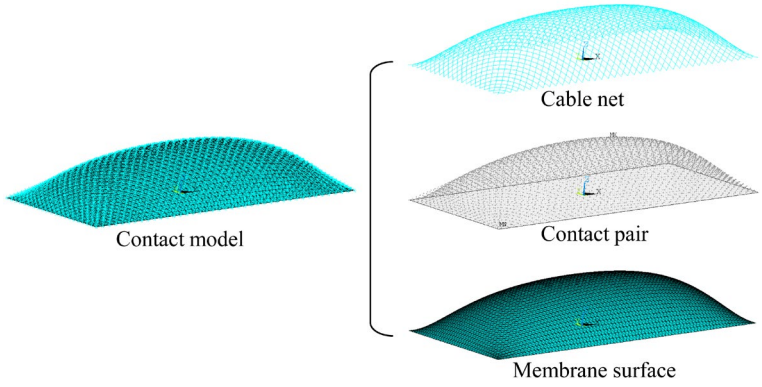

Figure 6 Contact model

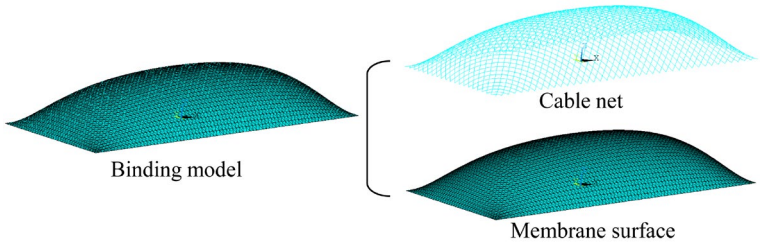

Figure 7 Binding model

In this study, the operational internal pressure of the air-supported membrane structure is established at 300Pa. According to Li's research [10], the friction coefficient between the cable and the membrane is 0.2. The additional material parameters utilized in the FE model are delineated in Table 1.

Table 1 Material parameters of the FE models

Parameter of membrane		Parameter of cable	
Membrane thickness	1mm	Cable diameter	22mm
Young's modulus	1.35×10^{9}N/m^2	Young's modulus	1.6×10^{11}N/m^2
Poisson's ratio	0.35	Poisson's ratio	0.3
Areal density	1000kg/m^3	Density	7850kg/m^3

4. The influence of cable-membrane contact on the static performance of air-supported membrane structures

This section examines the effect of cable-membrane contact on the static performance of air-supported membrane structures. Since wind load is the primary load, only wind load is considered, excluding other loads such as self-weight and snow load. The basic wind pressure is set at 500Pa, approximately 28.28m/s. Utilizing the mean wind pressure coefficient obtained from rigid model wind tunnel tests, the structure's wind loads are calculated and applied to the FE models. The focus is primarily on the structural responses such as displacement, stress, and support reactions of the cable and membrane, as well as the phenomena of cable-membrane relative slippage and separation. The structural global coordinate system is established as shown in Figure 8 to facilitate the description of structural responses. All subsequent references to the X, Y, and Z directions are predicated upon this coordinate system.

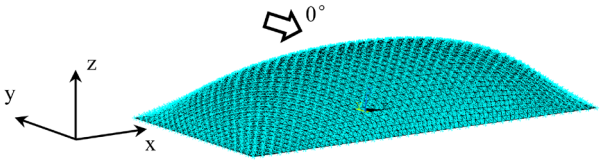

Figure 8 Structural global coordinate system

4.1 Displacement response

The membrane displacement contour in the Y and Z directions for both models is presented in Figure 9.

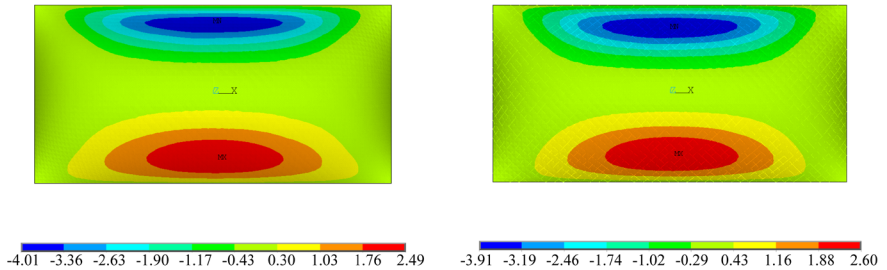

a) Y-displacement(Contact model) b) Y-displacement(Binding model)

c) Z-displacement(Contact model) d) Z-displacement(Binding model)

Figure 9 Membrane displacement contour

It is observable that the displacement distribution patterns of both models are remarkably similar, characterized by inward concavity in the windward area caused by wind pressure and upward bulging at the top caused by wind suction, which in turn induces inward movement in the leeward area. However, the membrane displacement in both directions in the windward area is greater for the contact model than the binding model.

4.2 Stress response

This section compares the stress distribution of the membrane and cable net between the two FE models, as shown in Figure 10.

The stress distribution of the two models is discernibly distinct. The maximum stress values for the membrane and cable net in the contact model are 309MPa and 514MPa, which are notably lower than those in the binding model, at 369MPa and 772MPa. Observing the overall distribution pattern, the stress distribution across the membrane and the cable net in the contact model is more uniform. This uniformity is attributed to the relative slippage that can occur between the cable net and the membrane in the contact model, preventing stress concentration in certain elements due to excessive constraints between the two components.

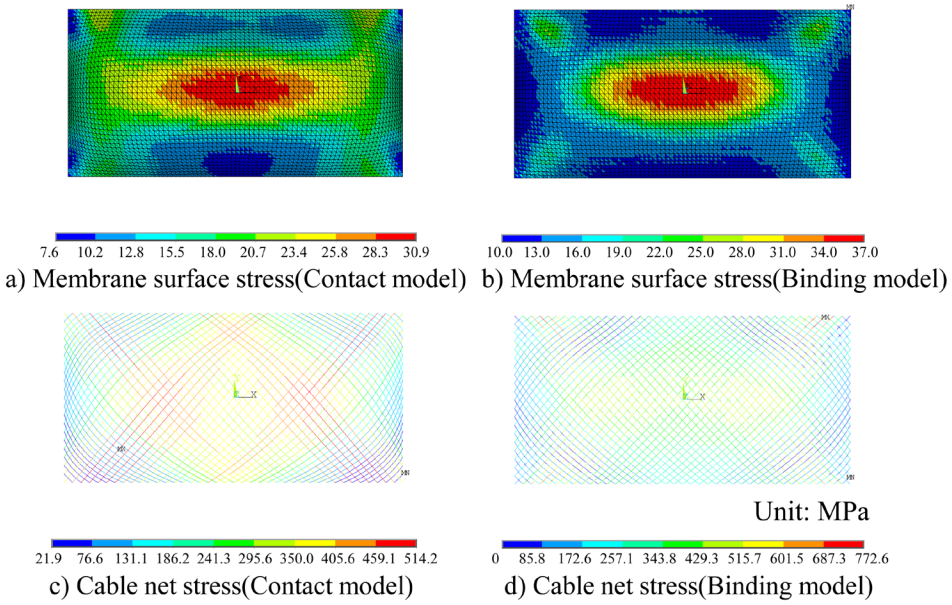

a) Membrane surface stress(Contact model) b) Membrane surface stress(Binding model)

c) Cable net stress(Contact model) d) Cable net stress(Binding model)

Figure 10 Membrane and cable net stress contour

In addition, key locations on the membrane and cable net are selected for a more detailed analysis. For the membrane, the path N-N' along the longitudinal axis at the mid-span is chosen to study the characteristics of the membrane stress variation along this path. Regarding the cable net, Cable1 where the maximum stress element in the contact model is located, is selected for examination. The study compares the variation in cable stress along this cable, as shown in Figure 11.

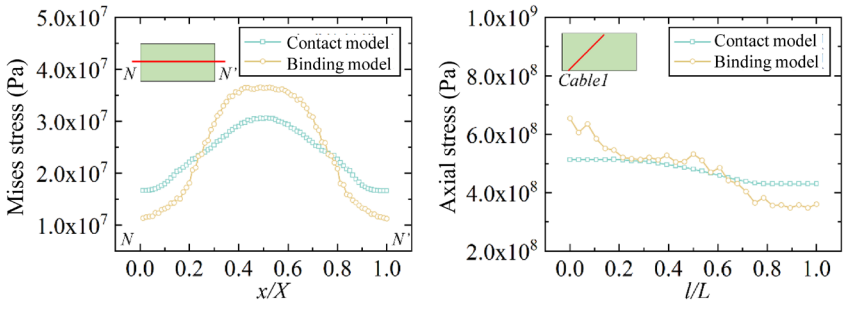

a) Membrane surface stress of path *N'-N'* b) Axial stress of *cable1*

Figure 11 Stress changes at key locations

The stress variation along the path N-N' is markedly distinct between the two models. In the contact model, the variation is relatively minor, with the minimum value being approximately 16.5MPa, occurring at both ends of the path N-N', and the maximum value around 30MPa, located at the midpoint. The membrane stress changes linearly, and the variation curve along the path forms an inverted V-shape. In contrast, the variation in membrane stress for the binding model is significantly greater than that of the contact model, with the minimum value at about 11MPa and the maximum reaching approximately 40MPa. The trend of stress variation also differs; the rate of increase in membrane stress from the ends to the midpoint of path N-N' first accelerates and then decelerates, resulting in an inverted U-shaped curve along the path.

The axial stress distribution in Cable 1 reveals a stark contrast between the two models. In the contact model, the variation in axial stress is smooth and continuous, with minimal fluctuation throughout the cable, closely resembling the actual state of stress. Conversely, in the binding model, adjacent elements may exhibit significant stress differences, with stress levels fluctuating, increasing and decreasing erratically, and the maximum stress value even reaches more than 3 times the minimum stress value, which evidently does not align with realistic conditions.

4.3 Support reaction response

The distribution of support reactions is discussed, as shown in Figure 12. The maximum support reaction forces on the membrane in both models are comparable, approximately 78kN. However, the distribution pattern differs slightly, with the support reaction forces at the two shorter edges of the contact model being significantly greater. The cable net support reaction primarily occurs on the two longer edges; however, there is a significant discrepancy between the support reaction values of the two models. The maximum support reaction force of the binding model reaches 300.2 kN, which is 1.5 times that of the contact model.

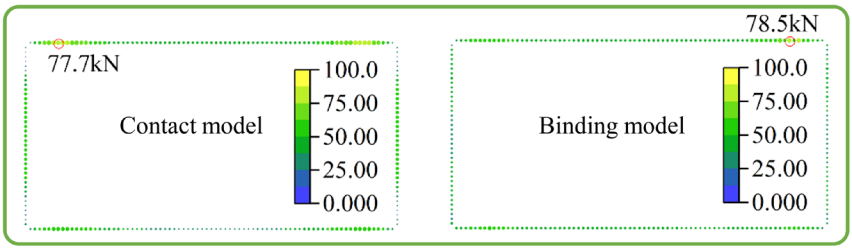

a) The support reaction of the membrane surface

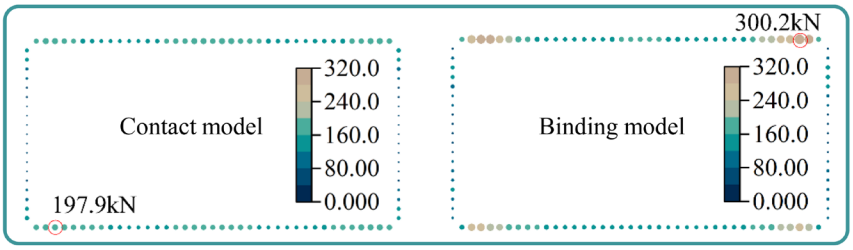

b) The support reaction of the cable net

3

Figure 12 Distribution of support reactions

The study also compiled the total support reaction forces of the membrane surface and the cable net for both models, along with their respective proportions, as shown in Table 2. The data reveals that the proportion of cable net support reaction in the contact model is lower than that in the binding model. This indicates that the binding model, which treats the cable and membrane as a unified entity, overestimates the wind load transferred from the membrane to the cable net and consequently overestimates the cable net's role in enhancing the aerodynamic stability of the air-supported membrane structure.

Table 2 Cable and membrane support reaction and their proportion

FE model	Support reaction of the membrane	The proportion of membrane	Support reaction of the cable	The proportion of cable
Contact model	11130.76kN	41.24%	15862.65kN	58.76%
Binding model	10479.02kN	37.67%	17337.84kN	62.33%

4.4 Cable-membrane separation phenomenon

To elucidate the phenomenon of cable-membrane separation, a side view of the structure's deformation is presented, and section 1-1 is selected to illustrate the relative positions of the membrane and cable net after deformation in the two FE models, as shown in Figure 13. It is observed that in the windward area,

the cable net of the contact model exhibits a pronounced separation from the membrane, with the membrane displacement significantly exceeding that of the cable net, resulting in a substantial gap. The displacement of the binding model is intermediate between the membrane and cable net of the contact model. This suggests that the binding model overestimates the restraining effect of the cable net on the membrane, and after the separation of the cable and membrane, the cable net's contribution to enhancing the wind resistance of the membrane structure is reduced.

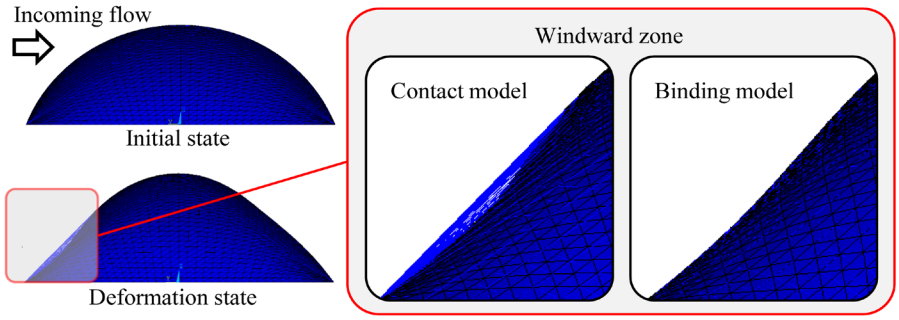

a) Deformed side view

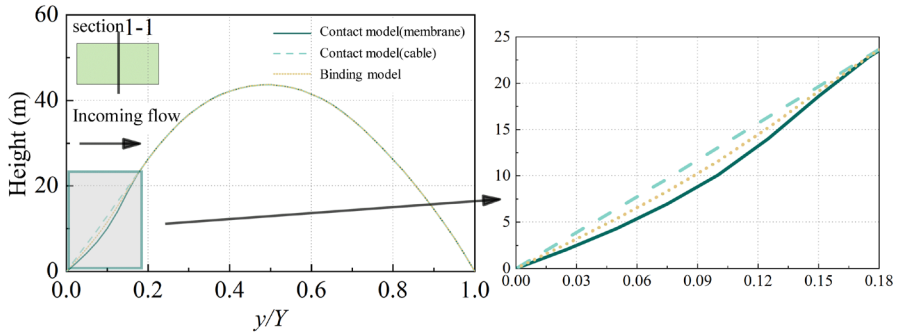

b) Relative position of cable and membrane in section1-1

Figure 13 Schematic diagram of cable-membrane separation

The maximum distance of cable-membrane separation serves as a key indicator for gauging the extent of separation. In this working condition, it is 1.28 meters. This parameter is predominantly influenced by the internal pressure (P) and wind pressure (w_0). By varying the internal pressure from 100 Pa to 500 Pa and the wind pressure from 100 Pa to 700 Pa, 28 distinct pressure ratio working conditions (w_0 / P) are established. The static analysis conducted on the 28 working conditions obtains the separation distances of the cable and membrane for each case, shown in Figure 14.

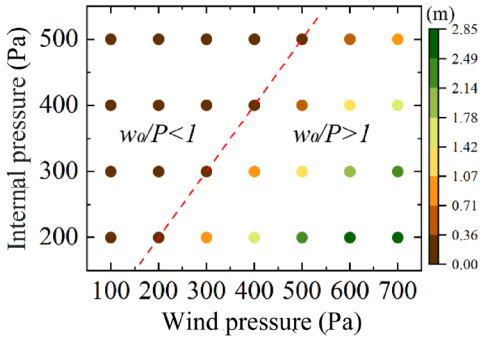

Figure 14 Cable-membrane separation distance

The red dashed line in the figure represents the boundary where the pressure ratio (w_0 / P) equals 1. In the region to the left, where the pressure ratio is less than 1, the maximum distance of cable-membrane separation approaches zero, indicating that separation is unlikely to occur. In contrast, the region to the right, where the pressure ratio exceeds 1, exhibits varying degrees of cable-membrane separation across

all working conditions. The maximum separation distance correlates positively with the pressure ratio. Notably, the working condition with an internal pressure of 200 Pa and wind pressure of 700 Pa obtains the greatest separation distance, reaching up to 2.85 meters.

5. Conclusion

The finite element analysis method for air-supported membrane structures that accounts for cable-membrane contact interactions has been established, enabling the simulation of cable-membrane separation and relative slippage phenomena. Based on the results of wind tunnel tests, the static wind response analysis conducted with the aforementioned analysis method has clarified the impact of cable-membrane contact on various static responses. Upon considering cable-membrane contact, the displacement of the membrane surface in the windward area increases, leading to cable-membrane separation. The maximum separation distance is positively correlated with the ratio of wind pressure to internal pressure (w_0 / P); it also diminishes the phenomenon of stress concentration, reduces the stress level in both cables and membranes and results in a more uniform and continuous change. Additionally, both the average level of the cable net and the proportion of total support reaction decrease. In summary, the binding treatment that does not consider the cable-membrane contact overestimates the reinforcing effect of the cable net on the air-supported membrane structures.

Acknowledgements

This work was supported by the National Natural Science Foundation of China (Grant No.52178134); and the Natural Science Foundation of Heilongjiang Province of China (No. LH2021E076).

References

[1] Y. Yin, W. J. Chen, J. H. Hu, B. Zhao, and Q. Wang, "In-situ measurement of structural performance of large-span air-supported dome under wind loads," *Thin-Walled Structures,* vol. 169, p. 108476, 2021-1-1 2021.

[2] X. Y. Li, Y. G. Wang, Q. Chu, S. D. Xue, and Y. L. He, "Wind-induced response monitoring of large-span air-supported membrane structure coal-shed under the influence of typhoons," *Thin-Walled Structures,* vol. 181, p. 109951, 2022-1-1 2022.

[3] Y. Wu, K. Y. Yan and Z. Q. Chen, "Aeroelastic wind tunnel investigations on rectangular-planed air-supported membrane structures," *Thin-Walled Structures,* vol. 190, p. 110955, 2023-1-1 2023.

[4] S. W. Zhang, "Study on wind tunnel test and wind resistance performance of rectangular plane air-supported membrane structure,": Harbin Institute Of Technology, 2021.

[5] Z. Q. Chen, J. B. Zhao and K. Y. Yan, "Wind tunnel test study on aero-elastic model of spherical inflatable membrane structures," *Journal of Building Structures,* vol. 44, pp. 137-147, 2023.

[6] Y. Fang, "Study on load effect of the cylindrical air-supported structure,": Xi'an University of Architecture and Technology, 2013.

[7] C. L. Xie, "Mechanics characteristic research on truncated-spherical inflatable membrane structure,": Xi'an University of Architecture and Technology, 2013.

[8] C. Wang, "Cable-membrane contact analysis of air-supported membrane structures,": Hefei University Of Technology, 2014.

[9] Y. L. He, M. X. Zhu, Y. G. Zhao, and X. Y. Li, "Influence of different cable–membrane connection models on wind-induced responses of an air supported membrane structure with orthogonal cable net," *Thin-Walled Structures,* vol. 180, p. 109840, 2022-1-1 2022.

[10] Z. J. Li, Y. Zhang, Y. G. Zhang, and Y. Xiang, "Experimental study on friction coefficients between membranes and cables," *Building Structure,* vol. 40, pp. 107-110, 2010.